PAPER

Encapsulation of γ-Fe₂O₃ decorated reduced graphene oxide in polyaniline core–shell tubes as an exceptional tracker for electromagnetic environmental pollution†

Avanish Pratap Singh,[ad] Monika Mishra,[a] Pradeep Sambyal,[a] Bipin Kumar Gupta,[b] Bhanu Pratap Singh,[c] Amita Chandra[d] and S. K. Dhawan*[a]

The ultimate goal of the development of a new material γ-Fe₂O₃ decorated reduced graphene oxide (rGO)–polyaniline (PANI) core–shell tubes has been done for absorbing electromagnetic interference (EMI) pollution. Herein, we report on the synthesis and characterization of PANI tubes consisting of rGO decorated with iron oxide nanoparticles (RF). The intercalated RF was synthesized by thermal decomposition of ferric acetyl acetonate in a reducing atmosphere. Furthermore, RF was encapsulated through oxidative polymerization of aniline in the presence of β-naphthalene sulphonic acid which results in RF–PANI core–shell morphology. Scanning electron microscopy results confirm the formation of tubular core–shell morphology having 5–15 μm length and 1–5 μm diameter. The presence of rGO–γ-Fe₂O₃ in PANI core enhances the interfacial polarization and the effective anisotropy energy of the composite which contributes to more scattering and leads to high shielding effectiveness ($SE_T \sim 51$ dB) at a critical thickness of 2.5 mm. Additionally, the effective complex permeability and permittivity parameters of the composites have been evaluated from the experimental scattering parameters (S_{11} & S_{21}) using theoretical calculations given in Nicholson–Ross and Weir algorithms.

1. Introduction

The recent advancement of electrical and electronic devices (TVs, computers, mobile phones, and radios *etc.*) has made human life easier, comfortable and luxurious. Simultaneously, the massive use of these devices generates a new kind of pollution known as electromagnetic interference (EMI). This electromagnetic (EM) pollution is not only adversely affecting the operation of electronic devices but is also harmful to the health of human beings. Due to this, EM wave absorbing materials have attracted much attention for the proper functioning of electronics, radio frequency radiation sources in all commercial, military equipment, scientific electronic devices, communication instruments and radiation sources. Also, the EMI shielding materials should be lightweight potential

absorbers of the radiation field to protect aircraft avionics and health hazards in humans. Therefore, in the last decades, a range of materials including very thin sheets of metals, different forms of carbon,[1,2] *e.g.*, graphite and its exotic forms[3,4] such as expanded graphite,[5] reduced graphene oxide (rGO),[6] carbon black,[7] graphene,[4] carbon fibers,[8,9] single or multiwalled carbon nanotubes (CNTs),[10] and conducting polymers, dielectric, magnetic materials and their composites have been used for EMI shielding in automotive applications. However, metals are expensive, heavy, and prone to corrosion, while adding to the complexity and cost of manufacturing processes. Therefore, as an alternative, intrinsically conducting polymer based composites with a wide range of electrical conductivity, permittivity (ε) or permeability (μ) have been suggested for microwave absorption. Thus, EM absorption properties of various polymer composites incorporated in dielectric or magnetic materials have been widely investigated. Among the nanostructures, conducting polymers, along with some magnetic and dielectric fillers, exhibit very good EM absorption properties.

Generally, the EMI shielding effectiveness (SE) of a material depends on its dielectric properties, magnetic permeability, thickness and frequency.[11] Techno-commercial applications such as, doppler, weather radar, TV picture transmission, and telephone microwave relay systems[12] require shielding in

[a]Polymeric & Soft Materials Section, CSIR-National Physical Laboratory, Dr K. S. Krishnan Road, New Delhi-110 012, India. E-mail: skdhawan@mail.nplindia.ernet.in; Fax: +91-11-25726938; Tel: +91-11-45609401

[b]Materials Physics and Engineering Division, CSIR-National Physical Laboratory, Dr K. S. Krishnan Road, New Delhi-110 012, India

[c]Physics and Engineering of Carbon, CSIR-National Physical Laboratory, Dr K. S. Krishnan Road, New Delhi-110 012, India

[d]Department of Physics & Astrophysics, University of Delhi, Delhi-110 007, India

† Electronic supplementary information (ESI) available. See DOI: 10.1039/c3ta14212d

This journal is © The Royal Society of Chemistry 2014

J. Mater. Chem. A, 2014, **2**, 3581–3593 | 3581

X-band (8.2–12.4 GHz) frequency range. The EMI SE of a composite is governed by intrinsic conductivity, aspect ratio, complex permittivity and permeability of the filler.[13] The primary mechanism of shielding is the reflection loss (SE_R) which is the result of interaction between the conducting particles in the conducting material (free electron or vacancy) and the EM field.[14] While the absorption loss depends on the value of σ_r/μ_r, i.e., the absorption loss is maximum when $\mu_r = \sigma_r$.[15,16] The high electrical conductivity,[17] high specific surface area (surface to volume ratio)[18] of graphene make it a unique candidate to provide remarkable EMI shielding[19] in polymer composites. Due to the sp^2 bonded carbon atoms, partially rGO has a good electrical response. Since graphene lacks in magnetic properties, it has only a small role in absorption of EM waves. In order to overcome this limitation, we have also synthesized nanoferrite particles on the rGO surfaces, which absorb more EM waves because of their large magnetic permeability.[20–23] Moreover, nanoferrite is not only environmentally friendly but also has an abundant natural supply, thus, rendering the material inexpensive.

Nowadays, graphitic materials have attracted the scientific and industrial community due to their potential applications in many areas, including EMI shielding. The graphene polymer composites are superior to CNTs polymer composites because these are more thermally stable, hold more stiffness, lower cost (compared to CNTs), and have the capability to form a thin film, paper or coating for EMI shielding and electrostatic charge dissipation (ESD) properties. The ultra-high thermal conductivity and lower density (four times as compared to copper) make graphene preferable for packing microelectronic devices in the form of a composite thin film, paper or coating. Our previous efforts based on graphene encourage us to search more and more a new kind of composites with graphene. The present investigation is one of the most innovative efforts to discover new kind of materials for EMI shielding.

To enhance the properties of conducting polymers for developing EMI shielding material, intensive efforts have been carried out on polymer ferromagnetic composites using Fe, Mn, Ni, Co ferrites and their multi-component ferrites like Fe_3O_4, Fe_2O_3, $BaFe_{12}O_{19}$, CrO_2, MnO_2, $Mn_{0.5}Zn_{0.5}Fe_2O_4$.[4,6,16,24–27] Among all of them γ-Fe_2O_3 is found to be the best for developing radar absorbing materials because it offers a high value of complex permeability.[27,28] Singh et al. have reported that super paramagnetic, nanocrystalline γ-Fe_2O_3 particles and its polymer composite show a M_s value of 69.0 and 20.56 emu g^{-1} at room temperature, respectively. The resulting conducting ferromagnetic composite shows microwave absorption loss of 22.8 dB.[27]

The manuscript reports synthesis of γ-Fe_2O_3 decorated rGO filled in a polyaniline (PANI) tube core–shell structure useful for microwave absorption. The selectivity of the different materials to synthesize the present composites has been based on systematic experimental efforts as well as the associated properties of these compounds to fabricate the desired material with all required properties for EMI shielding in a single composite.

Previously, PANI tubes have been synthesized by several other groups because of their great potential in device applications, such as transistors,[29] sensors,[30] and batteries.[31] PANI tubes have a diameter in the range of ~100 nm[32] and therefore there is a possibility to fill these tubes with materials like nanoferrite, rGO, rGO–nanoferrite. PANI tubes were filled with a mixture of rGO and γ-Fe_2O_3. β-Naphthalene-2-sulfonic acid (β-NSA) was used as a dopant and oxidant. A vibrating sample magnetometer (VSM) study of the composite sheets with different amounts of γ-Fe_2O_3 enabled us to understand their magnetic induction behavior and hence their effect on EMI shielding. The composite pellets having thickness critical 2.5 mm have shown high values of SE ranging from 21.49 to 53.83 dB (~99.99%) in the microwave range (X-band). Such novel composite may find potential applications such as EMI shielding, ESD, gas sensor etc.

2. Experimental

2.1. Materials

Aniline, ammonium persulfate (APS), hydrazine hydrate by Rankem Limited, India, Ferric acetylacetonate (Fe(acac)$_3$), methanol, H_2SO_4 by Merck, India, β-NSA by Himedia, HNO$_3$ by Fisher Scientific and natural graphite powder (purity 99.5%, particle size 50 μm) were procured from Loba Chemie, India. The aniline monomer was purified by distillation under reduced pressure before use. Aqueous solutions were prepared using doubly deionized water having a specific resistivity of 10^6 Ω cm. The other chemicals were of reagent grade and used as received.

2.2. Synthesis of rGO–γ-Fe_2O_3 incorporated polyaniline (PRF) composite

The chemical oxidative polymerization of aniline was carried out in the presence of γ-Fe_2O_3 decorated rGO (RF) particles to prepare PRF composites. Prior to PRF synthesis, in-situ synthesis of γ-Fe_2O_3 nanoparticles on the rGO matrix was carried out by taking 1 : 1 wt ratio of rGO and Fe(acac)$_3$ and the resultant composites were abbreviated as RF. The synthesis of RF and rGO were discussed in detail in our earlier report.[6] β-NSA was used as a dopant without an external template. This method belongs to a self-assembly process[12] because β-NSA works as a dopant and a template functioning at the same time. A typical preparation process for PANI-RF composite is as follows: 0.3 M solution of β-NSA and calculated amount of RF was homogenized (ART MICCRA D8 rotating at 17 600 rpm for 2 h) to obtain a uniform suspension containing RF particles. 0.1 M aniline was added and stirred continuously for another 1 h to form an emulsion. The aniline–β-NSA mixture containing RF particles were cooled in an ice bath for 2 h before oxidative polymerization. Finally, the oxidant APS (0.1 M) was added dropwise to the above solution. keeping the temperature of the reactor at 0 °C with vigorous stirring for 10 h. The green polymer precipitates thus obtained were treated with methanol in order to remove oligomers. The resulting precipitate was filtered and washed thoroughly until the filtrate became colorless and was then dried at 60–65 °C in a vacuum oven for 24 h. Throughout the experiment, the molar ratio of aniline to β-NSA and APS was retained at 1 : 3 and 1.0 respectively. However, the concentration of RF particles was changed to understand the effect of RF particles on the

3582 | J. Mater. Chem. A, 2014, 2, 3581–3593

This journal is © The Royal Society of Chemistry 2014

morphology, structure, electrical properties and shielding effectiveness of the resulting PANI–PRF composite tubes. Such a cooperative combination of β-NSA (non-corrosive organic dopant having surfactant traits), RF nanoparticles (conducting, magnetic and dielectric filler or guest) and PANI (electrically conducting matrix or host), can offer advantages such as good electrical, magnetic and dielectric properties which may collectively contribute towards high microwave absorption efficiency. Several compositions having different AN : RF weight ratios, *i.e.*, 1 : 0, 1 : 1, 1 : 2 and 1 : 3, were prepared and designated as PRF10, PRF11, PRF12 and PRF13, respectively.

2.3.   Materials characterization

The morphology of PANI–β-NSA tubes and its composites were examined using scanning electron microscopy (SEM, Zeiss EVO MA-10). The SEM samples were prepared by dispersing the powder in iso-propanol using ultra-sonication and placing small drops of the suspension on silicon wafers and sputter-coated with gold before analysis. High-resolution transmission electron microscopy (HRTEM) performed using Technai G20-stain 300 kV instrument. The semi-crystalline nature of PANI–β-NSA and PRF composite was confirmed by X-ray diffraction (XRD) studies[13] carried out on D8 Advance XRD (Bruker) using Cu Kα radiation ($\lambda = 1.54$ Å) in the scattering range (2θ) of 10–70° with a scan rate of 0.02° s^{-1} and a slit width of 0.1 mm. The electrical conductivity of PRF composites was examined by a well established four-probe method using a computer controlled Keithley current source (Model 6221) and nano-voltmeter (Model 2182A) at room temperature. For electrical conductivity measurements, rectangular pellets (13×7 mm^2) were prepared from a powder sample using rectangular die and hydraulic press at a compression pressure of 5 ton. Four ohmic contacts were made on the corners of a pellet using silver epoxy paste. The thermal stability of the composite was performed with a thermogravimetric analyzer (Mettler Toledo TGA/SDTA 851^e)[13] under inert atmosphere (flowing N$_2$ gas) in a temperature range 25–900 °C. FTIR spectra were recorded on Nicolet 5700 in transmission mode in the wavenumber range 400–2000 cm^{-1}. The spectroscopic grade KBr pellets were used for collecting the spectra with a resolution of 4 cm^{-1} performing 32 scans. Raman analysis was carried out using Renishaw in Via Reflex spectrometer, UK with an excitation source of 514.5 nm. The resolution of the instrument was less than 1.0 cm^{-1}. To explore the EMI shielding dielectric measurements of the composite Agilent E8362B Vector Network Analyzer was used in the X-band. The Powder samples were pelletized in a rectangular shape with dimensions 22.8×10 mm^2 of thickness ∼2 mm and inserted into a copper sample holder connected between the wave-guide flanges of a network analyzer.
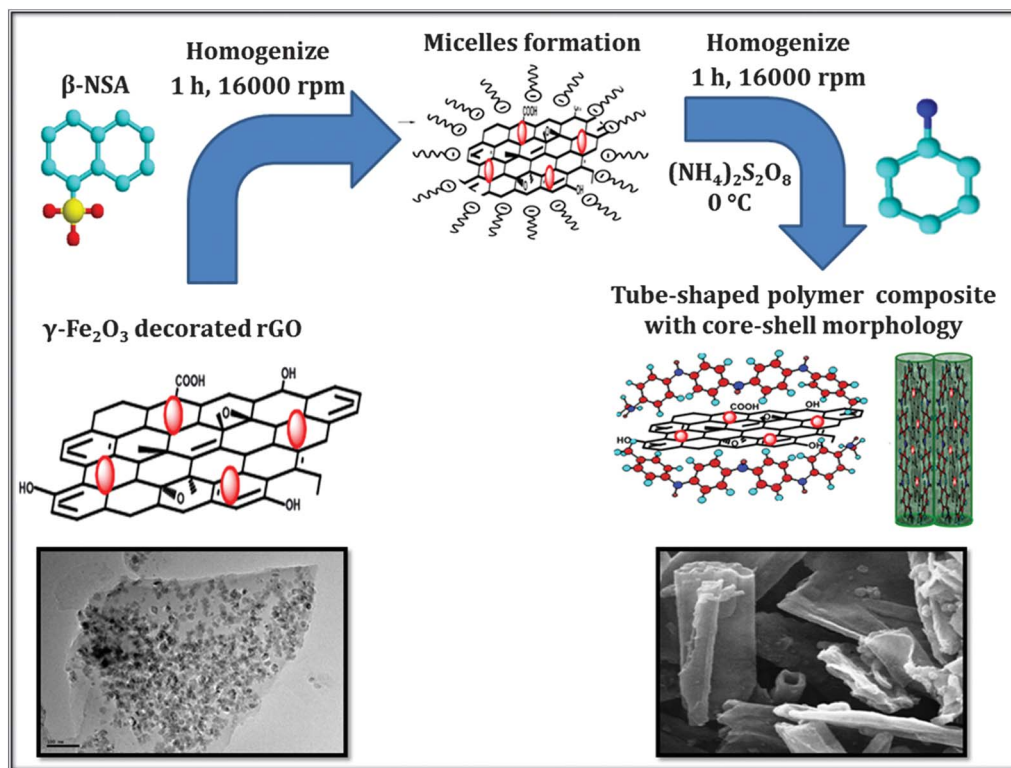
3.   Results and discussion

The RF filled PANI nanocomposites (PRFs) were prepared by *in situ* emulsion polymerization using β-NSA as an anionic surfactant molecule which also acts as a dopant. Due to its amphiphilic and surfactant nature, the β-NSA molecule (with hydrophilic SO$_3$H head and hydrophobic tail) easily forms micelles in aqueous solution. As discussed in the Experimental section, RF particles were dispersed in β-NSA aqueous solution before polymerization. As a result, micelles containing RF particles form in the reaction, these micelles have a core–shell structure. 0.1 M aniline monomer was added to the above emulsion and homogenized for another 1 h. During this, aniline reacts with β-NSA to form aniline–β-NSA micelles which act as a soft template with formation of oil in a water type emulsion. Afterwards the homogenized mixture was transferred to a double-walled glass reactor, pre-cooled to −5 °C. Polymerization was initiated by dropwise addition of a water soluble oxidant, *i.e.*, APS and allowed to continue at −5 °C under continuous stirring. During this process the formed anilinium cations might be absorbed on the plane of these core–shell micelles. Furthermore, free aniline present in the solution might diffuse into the micelles to form aniline-filled micelles. Therefore, these micelles (with or without RF) act as soft templates for the formation of a tube-like structure. The attached –SO$_3$H groups impart an additional dopant property to β-NSA. As the polymerization advances, the micelles containing RF particles would become bigger spheres and take the shape of tubes/rods by elongation. Therefore, subsequent oxidation of aniline results in radical cations which combine with another unit to form a neutral dimer. Further oxidation of the dimer leads to the formation of a trimer, tetramer and finally the formation of polymer composites. Scheme 1 discussed a self-assembly process resulting in a tube-like structure of PANI and PRFs composites[33,34] and suggests that RF particles should be situated inside the polymer tubes. Schematic representation of the incorporation of RF into PANI matrix is given in this scheme which suggests that rGO and γ-Fe$_2$O$_3$ embedded in PANI tubes leads to the formation of PANI composites which has better electrical and magnetic properties. The presence of rGO containing iron oxide nanoparticles in a polymer matrix was confirmed by XRD of the composites. The presence of γ-Fe$_2$O$_3$ magnetic nanoparticles in the RGO matrix was confirmed by TEM.

3.1.   SEM analysis

SEM was carried out to determine the distribution of rGO or rGO platelets and γ-Fe$_2$O$_3$ in the polymer matrix. Fig. 1(a) shows agglomerated magnetic nanoparticles derived from the thermal decomposition of Fe(acac)$_3$. The estimated particle size of rGO was found up to few micrometers as shown in Fig. 1(b), although the thickness of rGO sheets and particle size of γ-Fe$_2$O$_3$ have not been possible to explore *via* a SEM technique. The inset shows the distribution of nanoparticles of γ-Fe$_2$O$_3$ on the surface of a rGO sheet. A SEM image of PANI composites synthesized in the presence of β-NSA reveals an interesting morphology featuring formation of a tube-like structure (Fig. 1(c)). Densely packed tubes have a range of diameters and lengths of ∼0.5 to 2 μm and up to 15 μm, respectively. A SEM micrograph of PANI composites reveals that RF particles are entrapped within the PANI matrix (Fig. 1(d)). This reduces the length of the tubes and increases the roughness of the surface. The diameter of the PANI composite is larger than the pristine PANI.

This journal is © The Royal Society of Chemistry 2014

J. Mater. Chem. A, 2014, **2**, 3581–3593 | 3583

Scheme 1 Schematic representation of the fabrication of γ-Fe$_2$O$_3$ nanoparticles decorated rGO sheets filled in PANI tubes by *in situ* polymerization of aniline using APS as oxidant in the presence of β-NSA.

3.2. TEM analysis

Fig. 2 demonstrates TEM/HRTEM images of γ-Fe$_2$O$_3$, rGO sheet, RF, pristine PANI and PANI composites. Fig. 2(a) shows iron oxide nanoparticles derived from Fe(acac)$_3$ by thermal decomposition at 186 °C in an organic solvent. The lattice plane spacing of the γ-Fe$_2$O$_3$ particles is about 0.29 nm which corresponds to the (206) plane as shown in Fig. 2(b). This was first confirmed using the XRD pattern of the γ-Fe$_2$O$_3$ phase. Fig. 2(c) shows an HRTEM image of a few rippled rGO nanosheets which clearly indicates the graphitic lattice. The interplanar distance was measured to be 0.37 nm, corresponding to the spacing of the 002 planes. This is consistent with the result calculated from XRD analysis, Fig. 3(a). The dispersion of γ-Fe$_2$O$_3$ in the rGO matrix is confirmed by the HRTEM image (Fig. 2(d)). Fig. 2(e) shows the PANI tubes having diameter ~1.75 μm and length ~6 μm. The PANI tubes are filled with a mixture of nanoferrite particles and rGO. The diameter of the PANI composite is more comparable to the pristine PANI tubes (Fig. 2(f)). The presence of rGO (conducting filler) and γ-Fe$_2$O$_3$ nanoparticles (magnetic filler) in the core of PANI is helpful for improving the matching of ε_r and μ_r which is necessary for enhancing the absorption of the EM wave.

3.3. XRD analysis

Fig. 3(a) shows the XRD patterns of γ-Fe$_2$O$_3$, RF, pristine PANI, and PANI composite. The main peaks for γ-Fe$_2$O$_3$ are observed

at $2\theta = 30.265°$ ($d = 2.9530$ Å), $2\theta = 35.659°$ ($d = 2.5177$ Å), $2\theta = 43.320°$ ($d = 2.0886$ Å), $2\theta = 57.321°$ ($d = 1.6073$ Å) and $2\theta = 62.981°$ ($d = 1.4758$ Å) corresponding to the (2 2 0), (3 1 1), (4 0 0), (5 1 1) and (4 4 0) reflections, respectively. All observed peaks of γ-Fe$_2$O$_3$ were matched with the standard XRD pattern (Powder Diffraction File, JCPDS no. 39-1346). The peaks present in γ-Fe$_2$O$_3$ were also observed in iron incorporated rGO composite sheets which indicates the presence of ferrite particles in the rGO matrix. The presence of rGO is confirmed by the broad peaks at $2\theta = 26.441°$ ($d = 3.368$), $2\theta = 54.599°$ ($d = 1.679$ Å). PANI shows two broad peaks at $2\theta = 19.795°$ ($d = 4.481$ Å) and $25.154°$ ($d = 3.537$ Å), which reveals its amorphous nature.[33] The peaks of RF observed in PRF13 confirm the presence of a RF hybrid in the polymer matrix. The crystallite size of γ-Fe$_2$O$_3$ particle can be calculated by using the Debye Scherrer formula, $D = k\lambda/\beta\cos\theta$, where D is the crystalline size, λ the X-ray wavelength, K the shape factor, θ the half angle in degrees, and β the line broadening measured by half-height in radians. The value of k is often assigned a value of 0.89, which depends on several factors, including the Miller index of the reflecting plane and the shape of the crystal. The average size of γ-Fe$_2$O$_3$ particles was calculated using the above equation and estimated as 8.99 nm for pure γ-Fe$_2$O$_3$ and 9.83 nm for iron incorporated rGO. The peaks at $2\theta = 30.265°$ ($d = 2.9530$ Å), $2\theta = 35.659°$ ($d = 2.5177$ Å) for γ-Fe$_2$O$_3$ in the PANI composites show the formation of composites having separate phases of both compounds properly dispersed in the polymer matrix.
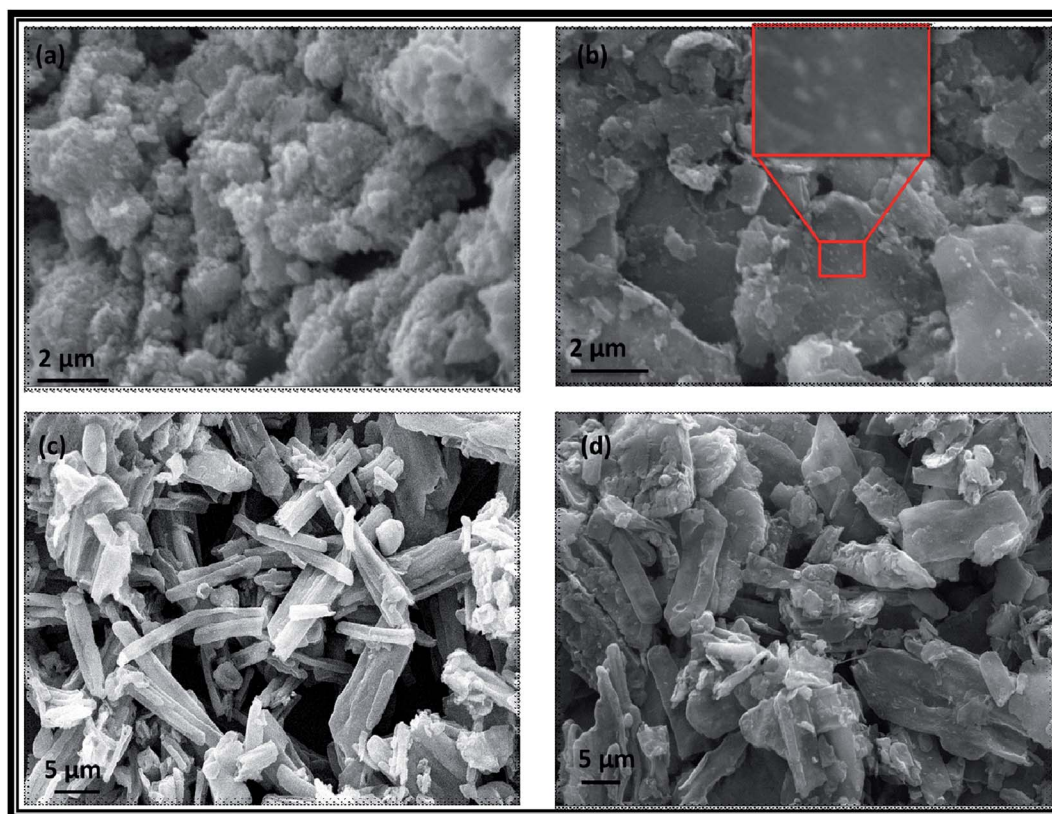
3584 | *J. Mater. Chem. A*, 2014, **2**, 3581–3593

This journal is © The Royal Society of Chemistry 2014

Fig. 1 SEM images of (a) iron oxide nanoparticles derived from Fe(acac)$_3$ by thermal decomposition at 186 °C, (b) reduced graphene oxide sheets decorated with γ-Fe$_2$O$_3$ nanoparticles, (c) PRF10 and (d) PRF13, showing the formation of a tube-like structure with RF particles inside the tubes.

3.4. TGA analysis

The TGA of the PANI doped with β-NSA and PANI composites was carried out in order to see the effect of the RF content on the thermal stability of the composite (Fig. 3(b)). Pure RF is thermally stable up to 303 °C and the weight loss was only 2%. The PANI composites show multi-step weight loss corresponding to the loss of different species. The first loss step at 120 °C is due to loss of water and other volatiles. The second loss in the range of 230–380 °C is due to loss of the –SO$_3$H functional group of the dopant and the onset of polymer degradation. The final major loss step (380° to 700 °C) is attributed to the complete degradation of the dopant as well as the polymeric backbone. The initial decomposition temperature (IDT) where degradation reactions first started, was also affected by increasing the RF content. The PANI doped with β-NSA (PRF10) was found to be thermally stable up to 237 °C. However, when the conducting polymer was synthesized by incorporating RF in (PRF11), it was observed that the thermal stability of the polymer increased to 273 °C. This shows that *in situ* polymerization of aniline in the presence of RF particles leads to a more thermally stable conducting polymer. The approximate amount of incorporated RF in composites was calculated by subtracting the wt% char residue (at 900 °C) of the blank polymer from that of the respective composites. It was observed that in the four different compositions, PF10; PF11; PF12 and PF13; the wt% of RF were estimated to be 0, 20.17, 43.15 and 60.55% which are in accordance with the amount taken during synthesis.

3.5. Magnetic properties

The field dependence of magnetization for the PANI composite containing different wt% of rGO decorated with γ-Fe$_2$O$_3$ nanoparticles was studied using the M–H curve at room temperature, as shown in Fig. 3(c). The saturation magnetization (M_s) value of the γ-Fe$_2$O$_3$ was found to be 29.15 emu g^{-1} at an external field of 5 kOe having a small value of coercivity and negligible retention with no hysteresis loop, indicating a super paramagnetic nature. When these nanoferrite particles are incorporated in the rGO matrix in 1 : 1 weight ratio, the M_s value was found to be 16.25 emu g^{-1}. Furthermore, it is expected that M_s value may greatly decrease for PANI composites (*e.g.* in PRF11 the M_s value decreases from 16.25 to 2.47 emu g^{-1}) because iron oxide is encapsulated in the polymer tubes. The role of the tube thickness is important to control the sufficient magnetization value which is required for EMI shielding applications. We have done several trials to optimize the polymer concentration in the composite to control the magnetization, efficient capping as well as optimum conductivity for shielding the application M_s values of different PANI composites were measured and given in Table 1 (see ESI†). The ferromagnetic properties of the composites further confirm that the oxide in the present investigation is γ-Fe$_2$O$_3$ rather than Fe$_3$O$_4$ which is also supported by the XRD pattern. The M_s value of PANI composite increases with the increase of RF loading due to the higher content γ-Fe$_2$O$_3$.

This journal is © The Royal Society of Chemistry 2014

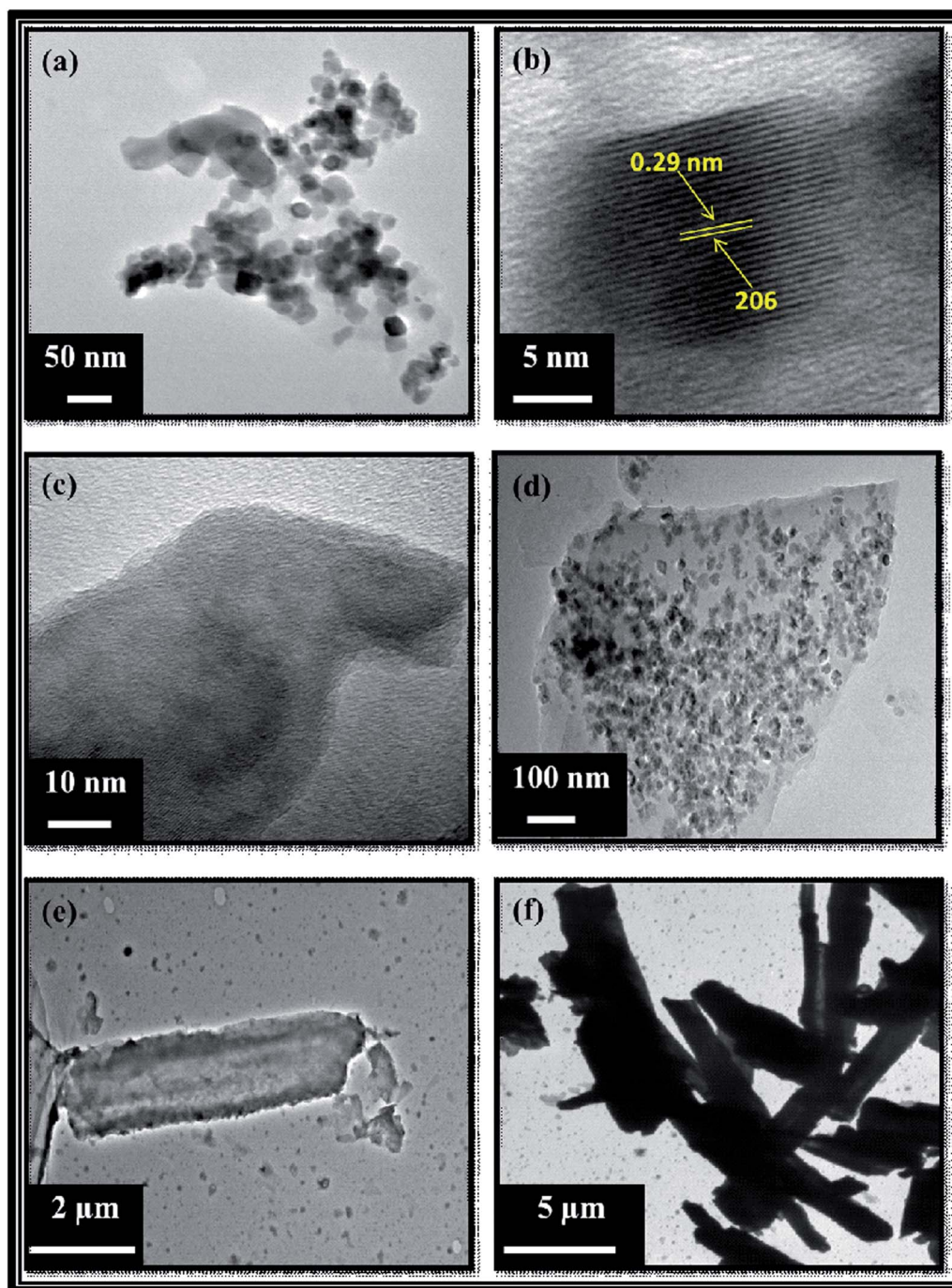*J. Mater. Chem. A*, 2014, **2**, 3581–3593 | **3585**

Fig. 2 (a) TEM image of γ-Fe_2O_3, (b) high magnification HRTEM image of γ-Fe_2O_3 showing the (206) oriented lattice planes of γ-Fe_2O_3, (c) TEM image of rGO sheets, (d) TEM image of rGO–γ-Fe_2O_3 hybrid structure, showing the nanoparticles of γ-Fe_2O_3 on the rGO surface, (e) TEM micrographs of pristine PANI tube and (f) PANI tubes filled with a mixture of rGO–γ-Fe_2O_3.

3.6. FTIR spectroscopy

Fig. 3(d) demonstrates the FTIR spectra of GO, rGO, RF, PRF10, PRF11, PRF12, and PRF13. The spectrum of GO shows the presence of various oxygen-containing functional groups; characteristic peaks at 1725 and 1105 cm^{-1} were assigned to C=O from carboxyl (COOH) and (C–O–C) groups from epoxide, respectively. The peak at 1630 cm^{-1} arises due to the contributions from the skeletal vibrations of unoxidized graphitic domains or the remaining sp^2 carbon character of graphite (C–C). However, in the case of RGO, RF and PANI composites, most of the oxygen-containing functional groups decrease or disappear which confirms the efficient reduction of GO. In the FTIR spectra of PANI (PRF10), bands near 1460 and 1570 cm^{-1} are assigned to the C=C stretching of the benzenoid and quinoid rings, respectively. The peak at 1300 cm^{-1} is assigned to the C–N stretching of the secondary amine, a characteristic
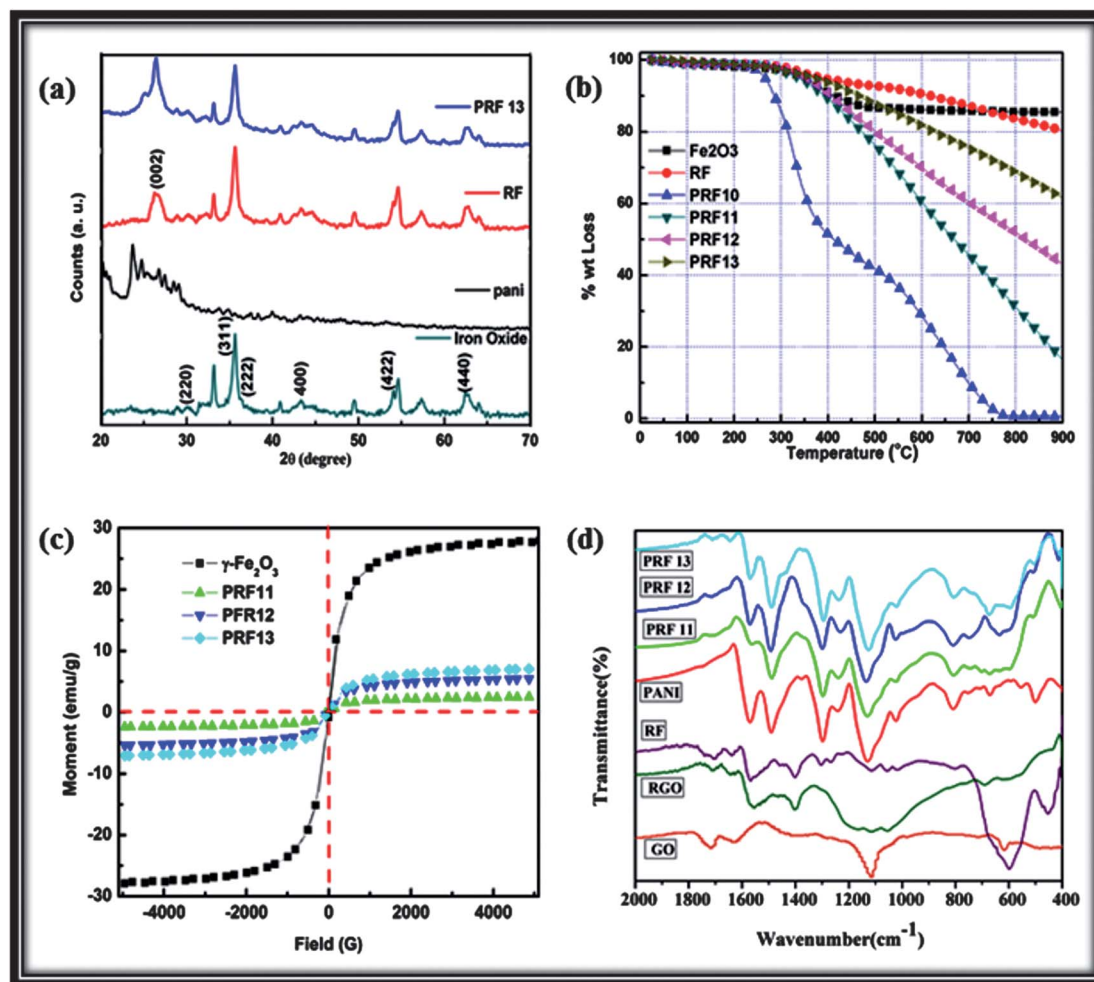
Fig. 3 (a) XRD of γ-Fe_2O_3, pristine PANI, RF and PRF13, (b) thermogravimetric (TG) plots of PANI–RF composites with different RF contents in N_2 atmosphere, (c) vibrating sample magnetometer plots of γ-Fe_2O_3 and PANI composites (d) comparison of FTIR spectra of GO, rGO, RF, PRF10, PRF11, PRF12, and PRF13.

band of the conducting emeraldine salt form of PANI originating from a bipolaron structure related to the C–N stretching vibration. The band at 1130 cm^{-1} can be assigned to an in plane bending vibration of the C–H (mode of N=Q=N, Q=N$^+$H–B, and B–N$^+$H=B), which is formed during protonation. Hence, these FTIR spectra correspond to a well-doped emeraldine salt. The band at 670 cm^{-1} (Fe–O stretching) confirms the formation of γ-Fe_2O_3 on the graphene sheets.

3.7. Raman spectroscopy

Raman spectroscopy is an important tool for identifying the proper interaction or bonding between two components.[35] Fig. 4 shows the Raman spectra of RGO, RF, PRF10, and PRF13. The Raman spectra of RGO consist of three prominent characteristic peaks, namely D band, G band, and G′ (2D) band confirming the formation of RGO. The inset of Fig. 4 shows the Raman spectrum of pure γ-Fe_2O_3 which reveals all characteristic bands of γ-Fe_2O_3 in the low frequency region, *i.e.*, E_g mode (245, 294, 301, 422, 611), A_{1g} mode (513) confirming the presence of γ-Fe_2O_3.[36] A broad 2D peak due to the presence of RGO was observed in all

three spectra of RGO, RF and RF13 and a slight right shift in the peak position from RGO and RF to RF13 was also observed. The bands at 1167 and 1623 cm^{-1}, assigned to C–H, and C–C of benzenoid units, respectively, were observed in the PANI spectrum (PRF10).[37] The same bands were observed for PANI composites with a slight blue shift, *i.e.*, 1167 to 1172 cm^{-1} and 1623 to 1625 cm^{-1}. Another band at 1321 cm^{-1} related to C–N stretching modes of delocalized polaronic charge carriers which is characteristic of the protonated imine form of PANI,[38] was also observed. This band shifted to 1342 from 1321 cm^{-1} with the incorporation of RF. Slight shifting in the bands is an evidence of interaction between these components. In addition to this, the low frequency mode of γ-Fe_2O_3 was also seen in RF and PRF13 samples due to the presence of γ-Fe_2O_3 in the material.

3.8. Conductivity

The room temperature electrical conductivity of the composites (Table 1†) increases sharply on higher loading of γ-Fe_2O_3 decorated rGO, *i.e.*, from 21.49 S cm^{-1} (PRF10) to 53.83 S cm^{-1}
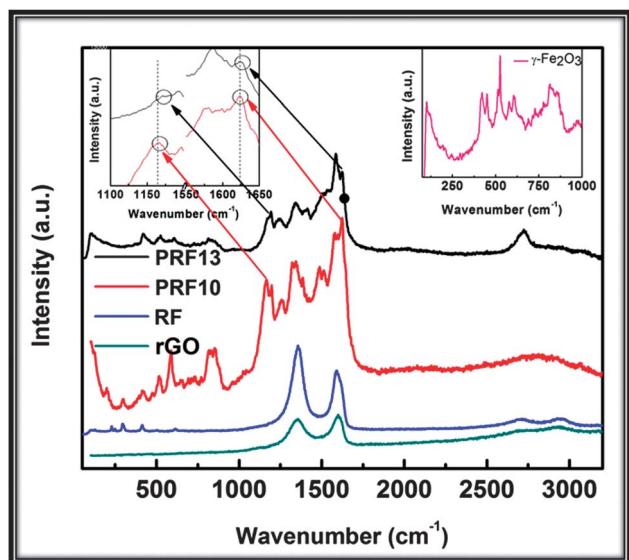
Fig. 4 Raman spectra of rGO, RF, PRF10, PRF13 and inset image shows the Raman spectra of γ-Fe_2O_3.

(PRF13). This is attributed to two reasons. Firstly, the rGO sheets possess very good conductivity. Secondly, the conducting network is improved on higher wt% loading of RF particles resulting in enhancement of the electrical conductivity of the composites. Most importantly, these samples show an optimum value of conductivity and magnetization which is desired for exhibiting good microwave shielding responses.[6,39]

3.9. Electromagnetic shielding and dielectric studies

The EM parameters, *i.e.*, relative complex permittivity ($\varepsilon^* = \varepsilon' - i\varepsilon''$) and relative complex permeability ($\mu^* = \mu' - i\mu''$) were measured at room temperature for the study of microwave absorption properties of PANI composites which are shown in Fig. 5(a)–(f). These obtained complex parameters were estimated from the experimental scattering parameters (S_{11} and S_{21}) by standard Nicholson–Ross and Weir theoretical calculations.[40]

The estimated real part of the EM parameters (ε', μ') is directly associated with the amount of polarization occurring in the material which symbolizes the storage ability of the electric and magnetic energy, while the imaginary part (ε'', μ'') signifies the dissipated electric and magnetic energy.

From Fig. 5(a), for PANI composites PRF11, PRF12 and PRF13, the values of ε' are in the range of 121.82–84.68, 206.94–130.93, and 339.45–233.77, respectively, which are higher than the pristine PANI (71.94–42.60) in the frequency range 8.2 to 12.4 GHz. Meanwhile, the values of ε'' for PRF11, PRF12 and PRF13, are in the range of 77.35–44.27, 129.60–82.58 and 166.28–74.39, respectively, which are also higher than pure PANI (41.78–36.35) as shown in Fig. 5(b). It is observed that samples with higher wt% loading of RF show higher values of ε' and ε'' due to higher conductivity of RF. It is proposed that more rGO plates may enhance conductivity and electric polarization because permittivity (ε') is a measure of the polarizability of a material which induces dipolar and electric polarization in the presence of microwave.

As shown in Fig. 5(c) for PANI composites PRF11, PRF12 and PRF13, the values of μ' are in the range of 0.69–0.70, 0.98 1.15 and 1.41–1.71, respectively, which are higher than pristine PANI (0.16–0.18) in the X-band. Meanwhile, the values of μ'' for PRF11, PRF12 and PRF13 are in the range of 0.09–0.05, 0.11–0.02 and 0.49–0.50 respectively, which are almost equal to pure PANI (0.08–0.02), as shown in Fig. 5(d). Dielectric tangent loss (tan $\delta_E = \varepsilon''/\varepsilon'$) and magnetic tangent loss (tan $\delta_M = \mu''/\mu'$) of PANI composites are also calculated using the permittivity and permeability parameters of the samples and are presented in Fig. 5(e and f respectively). The observed tan δ_E is always greater than 0.3 in the entire frequency range, indicating that dielectric loss occurs in all frequency ranges. These results suggest that PANI composites have distinct dielectric loss properties.

According to the EM theory, dielectric loss is the result of complex phenomena like natural resonance, dipole relaxation, electronic polarization and its relaxation, polarization of polarons and bipolarons in the polymer matrix and their relaxation and certainly the unique structure of the shield. Iron oxide nanoparticles decorated in rGO sheet, acts as a polarized centre inside the PANI tube which results in greater microwave absorption. The high aspect ratio of the PANI tubes filled with RF nanoparticles having high conductivity also enhances the absorption properties. In PANI composites, the existence of interfaces between iron oxide nanoparticles and rGO layer, iron oxide and PANI as well as between rGO and PANI is given. Ferromagnetic nanoparticles act as tiny dipoles which get polarized in the presence of EM field and result in better microwave absorption.

PANI and RF nanoparticles and between PANI–PANI tubes, are responsible for interfacial polarization which further contribute to dielectric losses. Interfacial polarization occurs in heterogeneous media due to accumulation of charges at the interfaces and formation of large dipoles. Fig. 5(b) shows that ε'' increases with higher wt% loading of RF, this is attributed to a conducting network formed by nanoferrite particles decorated rGO sheets. In addition, the conductivity of the samples is further improved by conducting PANI tubes, and results in the increase of dielectric loss. Moreover, dielectric loss is also improved by polaron and bipolaron hopping in the PANI matrix which has been reported earlier.[41] The magnetic loss (tan δ_M) is a result of eddy current effects, natural resonances and anisotropy energy present in the composites. In the microwave ranges, the presence of nanoferrite particles in the composite are the main cause of eddy current. The natural resonances in the X-band can be attributed to the small size of γ-Fe_2O_3 on the rGO sheet. Anisotropy energy of the small size materials,[42] especially in the nanoscale, would be higher due to the surface anisotropic field due to the small size effect.[43] The higher anisotropy energy also contributes in enhancement of the microwave absorption.

EMI SE of any material can be expressed as[4,6,25,27,41,44]

$$SE\ (dB) = SE_R + SE_A + SE_M = 10\log(P_T/P_I)$$
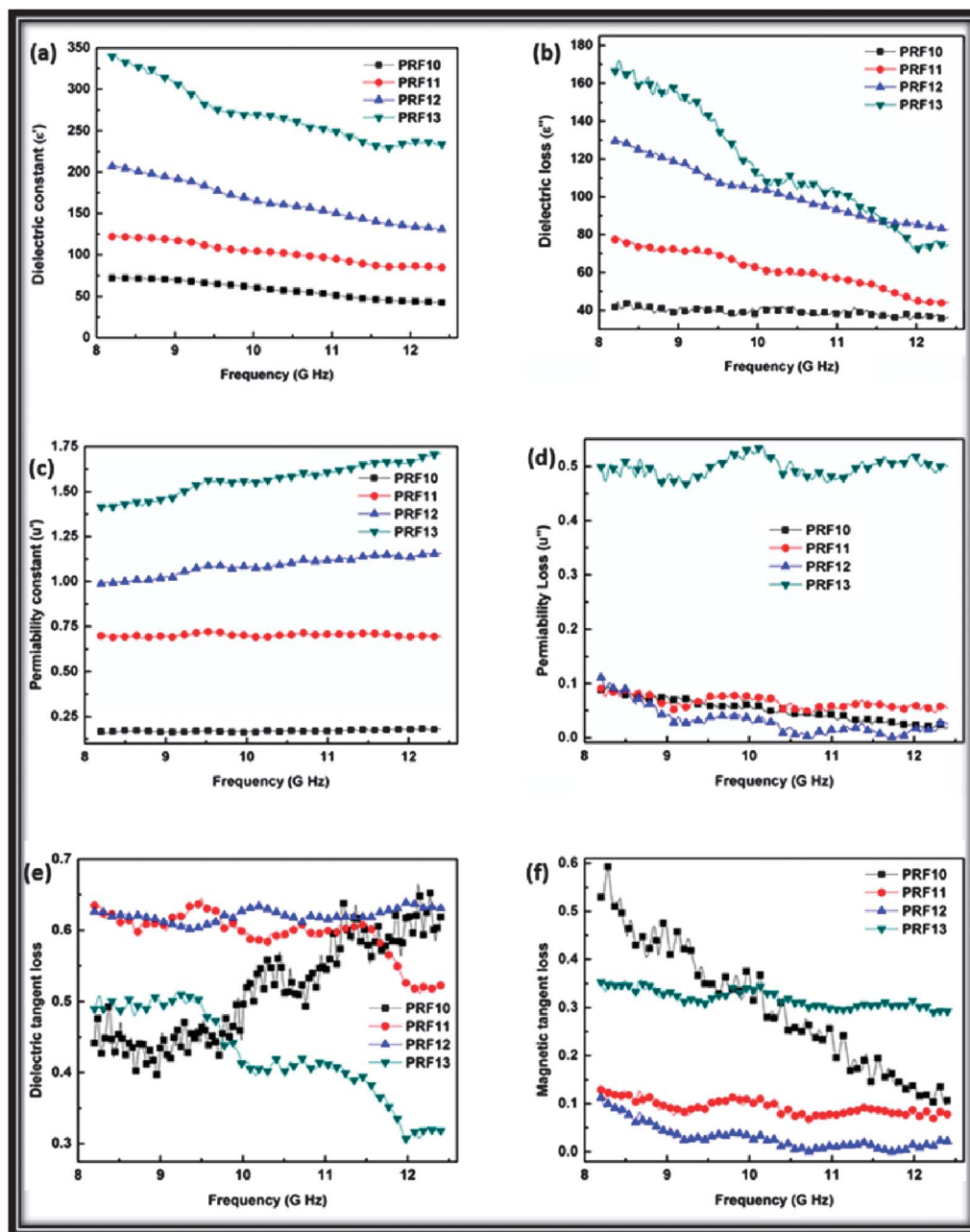$$= 20\log(E_T/E_I) \qquad (1)$$

Fig. 5 Frequency dependence of the (a) real parts and (b) imaginary parts of the complex permittivity, (c) real parts and (d) imaginary parts of permeability and the corresponding (e) dielectric loss tangents and (f) magnetic loss tangents of PANI composites.

where P_I (E_I) and P_T (E_T) are the power (electric field intensity) of incident and transmitted EM waves, respectively. The terms in eqn (1) can be defined as

$$SE_R = -10 \log(1 - R) \quad (2)$$

$$SE_A = -10 \log(1 - A_{eff}) = -10 \log(T/1 - R) \quad (3)$$

SE_R, SE_A and SE_M represents shielding effectiveness due to reflection, absorption and multiple reflections respectively. The correction term SE_M can be ignored in all practical application when SE > 10 dB.[45,46]

Therefore, the effective absorbance (A_{eff}) can be described as $A_{eff} = (1 - R - T)/(1 - R)$ with respect to the power of the effectively incident EM wave inside the shielding material.

For a material, the skin depth (δ) is the distance up to which the intensity of the EM wave decreases to $1/e$ of its original strength. The δ is related to angular frequency, relative permeability and total conductivity $\sigma_T = (\sigma_{dc} + \sigma_{ac})$. According to the EM theory, for electrically thick samples ($t > \delta$), the frequency (ω) dependence of the far field losses can be expressed in terms of total conductivity (σ_T), real permeability (μ'), skin depth (δ) and thickness (t) of the shield material as:[46]

This journal is © The Royal Society of Chemistry 2014

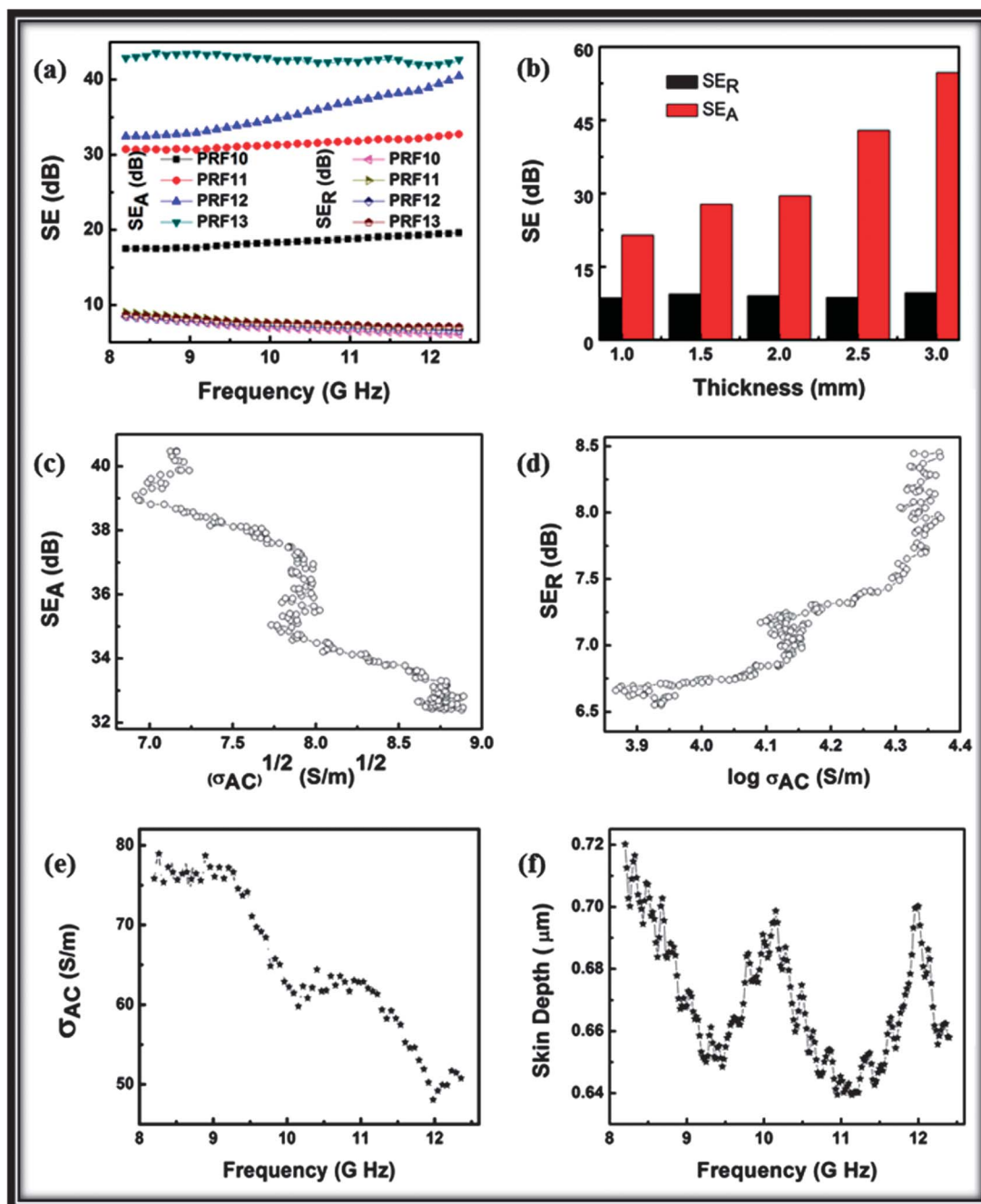*J. Mater. Chem. A*, 2014, **2**, 3581–3593 | **3589**

Fig. 6 (a) EMI SE of PANI composites having different wt% ratio of RF, (b) SE of PRF13 composite with different thickness, (c) dependence of SE_A as a function of $(\sigma_{ac})^{1/2}$ while (d) variation of SE_R as a function of $\log \sigma_{ac}$, (e) shows a variation of σ_{ac} with the increase in frequency and (f) shows change in skin depth with increase in frequency for sample PRF13.

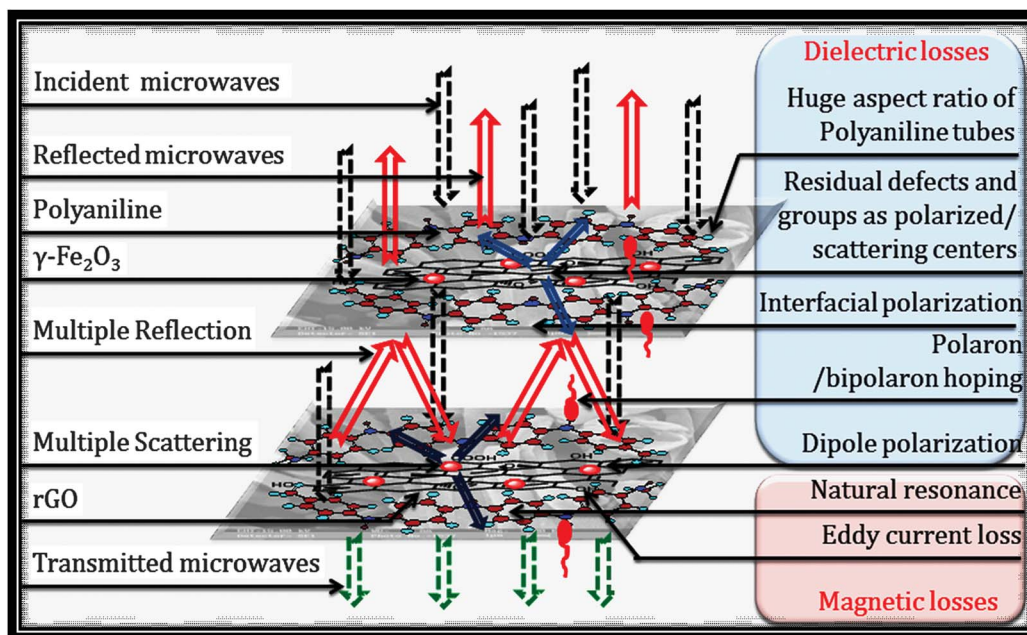$$SE_R \text{ (dB)} = 10 \log\{\sigma_{ac}/16\omega\varepsilon_0\mu'\} \qquad (4)$$

$$SE_A \text{(dB)} = 20\{t/\delta\}\log e = 20d\sqrt{\mu\omega\sigma_{ac}/2} \log e = 8.68\{t/\delta\} \qquad (5)$$

The σ_{ac} and δ can be related to the imaginary permittivity (ε'') and real permeability (μ') as $\sigma_{ac} = \omega\varepsilon_0\varepsilon''$ and $\delta = \sqrt{2/\sigma\omega\mu'}$ which gives absorption loss as:

$$SE_A \text{(dB)} = 8.68t\sqrt{\sigma\omega\mu'/2} \qquad (6)$$

SE_A becomes more dominant as compared to the SE_R in the microwave range. This may be caused by the shallow skin depth

and high conductivity (σ_{ac}) values at such high frequencies.[45,46] Fig. 6(a) shows the variation of the SE with frequency in the 8.2–12.4 GHz range. From the experimental measurement, the SE due to absorption (SE_A) of PANI composites was found to vary from 17 to 43 dB with increase in the γ-Fe_2O_3 content while the SE_R remains nearly constant at 9 dB. Thus, the total SE achieved for the composite is 51 dB (PRF13) which is higher than the pristine PANI (PRF10). It was observed that for conducting PANI composite, SE is mainly dominated by absorption while the SE_R is constant. It is observed that the thickness of the shield has a

3590 | *J. Mater. Chem. A*, 2014, **2**, 3581–3593

This journal is © The Royal Society of Chemistry 2014

Scheme 2 Schematic presentation of possible microwave absorbing mechanisms in the PANI composites.

great influence on the microwave absorbing properties as shown in Fig. 6(b). Our PANI composites exhibit better microwave absorption properties in comparison with pristine PANI,[33] pure rGO, γ-Fe$_2$O$_3$ nanoparticles,[47] PANI–γ-Fe$_2$O$_3$ composite,[47] PANI/multiwall carbon nanotubes composite,[48,49] PANI rGO iron oxide composites[50] reported earlier.

To relate σ_{ac} with the shielding parameter of the material, SE$_A$ has been plotted against $(\sigma_{ac})^{1/2}$, (Fig. 6(c)). The skin depth of the samples was calculated using the relation, $\delta = \sqrt{2/\omega\mu\sigma_{ac}}$ and its variation with frequency is shown in Fig. 6(f). It can be noticed that the skin depth is constant in the overall frequency range which demonstrates the surface conduction as shown in the figure exists in the whole frequency range. The skin depth of the PANI composite is very small (600 μm), due to the high electrical conductivity and good magnetic properties. From eqn (6), it can be seen that better SE$_A$ can be achieved from moderate conducting materials. The dependence of SE$_R$ as a function of log σ_{ac} is shown in Fig. 6(d) while Fig. 6(e) shows the variation of σ_{ac} with the increase in frequency for sample PRF13 calculated from the dielectric measurements ($\sigma_{ac} = \omega\varepsilon_0\varepsilon''$). Therefore, a moderate value of the conductivity (σ_{ac}) is required for materials having less SE due to reflection.

Reflection loss was also calculated from the experimental S parameter (S_{11}) using "Agilent E83628 PNA Vector Network Analyser". Measurements were performed according to Belaabed *et al.*[16] The wave guide is fitted with the sample backed by a metal short (see ESI†). The wave absorption property can be deduced from the measurement of the reflection loss RL (S_{11}) given by the network analyzer:

$$RL = 20 \log (S_{11})$$

The minimal reflection of microwave energy can be attributed to the dip in RL. It was observed that the composites

indicate a value of ~2.5 to 3.25 (dB) reflection loss at 10 GHz frequency. These results demonstrate that the intensity and frequency of the microwave energy absorption for the composite also depend on the rGO and iron oxide content in the PANI. Thus, microwave absorption properties of the composite are improved by the dielectric and magnetic losses. The reflection loss of PANI–rGO/iron oxide hybrid composites as a function of frequency at different filler's amount is given in the ESI.†

The excellent microwave absorbing performance of PANI composites is mainly attributed to two factors: impedance matching and EM wave attenuation. The ideal condition for the perfect absorber is $\varepsilon_r = \mu_r$, the presence of rGO sheet decorated with insulating magnetic γ-Fe$_2$O$_3$ nanoparticles in the core of the PANI matrix has lowered ε_r of the composite, and improved the equality of ε_r and μ_r, which helps the level of impedance matching.[16] Also, PANI composites have strong microwave absorption due to their dielectric and magnetic loss. Furthermore the high aspect ratio of PANI tubes, existence of residual defects in γ-Fe$_2$O$_3$ nanoparticles decorated rGO sheet[51] and multiple reflections in the shield enhance the microwave absorption ability of the composites. To further give a visual demonstration of the microwave absorption mechanism as discussed above, a schematic is given in Scheme 2. From all the above, the results of PANI composites illustrate that these composites could be used as a microwave absorbing material.

4. Conclusion

PANI micro-tubes filled with a mixture of rGO–γ-Fe$_2$O$_3$ were successfully synthesized using a microemulsion method which results in a core–shell tubular structure. The detailed microstructural/structural characterizations as well as the characteristics of these core–shell tubes were examined using SEM, TEM, XRD, FTIR, Raman, TGA and VSM. The core–shell tubular

This journal is © The Royal Society of Chemistry 2014

J. Mater. Chem. A, 2014, **2**, 3581–3593 | **3591**

structure associated with RF particles embedded in polymer chains attributes the enhanced interfacial polarization and the effective anisotropy energy of composite, and as a result more and more scattering occurs which leads to high SE (SE$_T \sim$ 51 dB) in comparison to conventional materials. The synthesized in-filled novel micro tubes have better microwave absorption properties (SE$_A \sim$ 43 dB) which strongly depend on optimal infilling of RF in the PANI matrix. Additionally, the microwave absorption properties can be tailored easily by varying the PANI–RF ratio and the thickness of the samples. Thus, the obtained results suggest that the PANI composite is a new promising microwave absorption material with vast utility in the radio frequency range maintaining strong absorption.

Acknowledgements

References

1 G. Tong, W. Wu, Q. Hua, Y. Miao, J. Guan and H. Qian, *J. Alloys Compd.*, 2011, **509**, 451–456.

2 T. GuoXiu, Y. JinHao, M. Ji, Q. M. Yue, G. J. Guo, L. L. Chao, G. PeiJun and C. JianJing, *Sci. Sin.: Chim.*, 2011, **41**, 1121–1126.

3 D. D. L. Chung, *Carbon*, 2001, **39**, 279–285.

4 A. P. Singh, M. Mishra, A. Chandra and S. K. Dhawan, *Nanotechnology*, 2011, **22**, 9.

5 M. Mishra, A. P. Singh and S. K. Dhawan, *J. Alloys Compd.*, 2013, **557**, 244–251.

6 A. P. Singh, P. Garg, F. Alam, K. Singh, R. B. Mathur, R. P. Tandon, A. Chandra and S. K. Dhawan, *Carbon*, 2012, **50**, 3868–3875.

7 N. C. Das, D. Khastgir, T. K. Chakia and A. Chakraborty, *Composites, Part A*, 2000, **31**, 1069–1081.

8 S. Yang, K. Lozano, A. Lomeli, H. D. Foltz and R. Jones, *Composites, Part A*, 2005, **36**, 691–697.

9 L. Li and D. D. L. Chung, *Composites*, 1994, **25**, 215–224.

10 A. P. Singh, B. K. Gupta, M. Mishra, Govind, A. Chandra, R. B. Mathur and S. K. Dhawan, *Carbon*, 2013, **56**, 86–96.

11 K.-Y. Park, J.-H. Han, S.-B. Lee, J.-B. Kim, J.-W. Yi and S.-K. Lee, *Compos. Sci. Technol.*, 2009, **69**, 1271–1278.

12 Y. Huang, N. Li, Y. Ma, F. Du, F. Li, X. He, X. Lin, H. Gao and Y. Chen, *Carbon*, 2007, **45**, 1614–1621.

13 N. Li, Y. Huang, F. Du, X. He, X. Lin, H. Gao, Y. Ma, F. Li, Y. Chen and P. C. Eklund, *Nano Lett.*, 2006, **6**, 1141–1145.

14 M. H. Al-Saleh and U. Sundararaj, *Carbon*, 2009, **47**, 1738–1746.

15 C.-S. Zhang, Q.-Q. Ni, S.-Y. Fu and K. Kurashiki, *Compos. Sci. Technol.*, 2007, **67**, 2973–2980.

16 B. Belaabed, J. L. Wojkiewicz, S. Lamouri, N. El Kamchi and T. Lasri, *J. Alloys Compd.*, 2012, **527**, 137–144.

17 S. Goswami, U. N. Maiti, S. Maiti, S. Nandy, M. K. Mitra and K. K. Chattopadhyay, *Carbon*, 2011, **49**, 2245–2252.

18 G. Eda and M. Chhowalla, *Nano Lett.*, 2009, **9**(2), 814–818.

19 X. Fu and D. D. L. Chung, *Cem. Concr. Res.*, 1996, **26**, 1467–1472.

20 Y. H. Jianfeng Shen, M. Shi, N. Li, H. Ma and M. Ye, *J. Phys. Chem. C*, 2010, **114**(3), 1498–1503.

21 H. He and C. Gao, *ACS Appl. Mater. Interfaces*, 2010, **2**(11), 3201–3210.

22 V. Chandra, J. Park, Y. Chun, J. W. Lee, I.-C. Hwang and K. S. Kim, *ACS Nano*, 2010, **4**, 3979–3986.

23 J. Liang, Y. Xu, D. Sui, L. Zhang, Y. Huang, Y. Ma, F. Li and Y. Chen, *J. Phys. Chem. C*, 2010, **114**, 17465–17471.

24 H. Xu, H. Zhang, T. Lv, H. Wei and F. Song, *Colloid Polym. Sci.*, 2013, **291**, 1713–1720.

25 A. Ohlan, K. Singh, A. Chandra and S. K. Dhawan, *J. Appl. Polym. Sci.*, 2008, **108**, 2218–2225.

26 R.-B. Yang, W.-F. Liang, W.-S. Lin, H.-M. Lin, C.-Y. Tsay and C.-K. Lin, *J. Appl. Phys.*, 2011, **109**, 07B527.

27 K. Singh, A. Ohlan, P. Saini and S. K. Dhawan, *Polym. Adv. Technol.*, 2008, **19**, 229–236.

28 X. Sun, J. He, G. Li, J. Tang, T. Wang, Y. Guo and H. Xue, *J. Mater. Chem. C*, 2013, **1**, 765–777.

29 B. H. Kim, D. H. Park, J. Joo, S. G. Yu and S. H. Lee, *Synth. Met.*, 2005, **150**, 279–284.

30 M. Kanungo, A. Kumar and A. Q. Contractor, *Anal. Chem.*, 2003, **75**, 5673–5679.

31 F. Cheng, W. Tang, C. Li, J. Chen, H. Liu, P. Shen and S. Dou, *Chem.–Eur. J.*, 2006, **12**, 3082–3088.

32 X. Lu, H. Mao, D. Chao, W. Zhang and Y. Wei, *J. Solid State Chem.*, 2006, **179**, 2609–2615.

33 A. P. Singh, A. K. S., A. Chandra and S. K. Dhawan, *AIP Adv.*, 2011, **1**, 022147.

34 J. C. Michaelson and A. McEvoy, *J. Chem. Soc., Chem. Commun.*, 1994, **79**, 79–80.

35 T. K. Gupta, B. P. Singh, S. R. Dhakate, V. N. Singh and R. B. Mathur, *J. Mater. Chem. A*, 2013, DOI: 10.1039/C3TA14854H.

36 S.-H. Shim and T. S. Duffy, *Am. Mineral.*, 2002, **87**, 318–326.

37 J. E. P. d. Silva, D. L. A. d. Faria, S. I. C. d. Torresi and M. L. A. Temperini, *Macromolecules*, 2000, **33**, 3077–3083.

38 A. Shakoor, T. Z. Rizvi and A. Nawaz, *J. Mater. Sci.: Mater. Electron.*, 2011, **22**, 1076–1080.

39 N. F. Colaneri and L. W. Shacklette, *IEEE Trans. Instrum. Meas.*, 1992, **41**, 291–297.

40 A. M. Nicolson and G. F. Ross, *IEEE Trans. Instrum. Meas.*, 1970, **19**, 377–382.

41 A. Ohlan, K. Singh, A. Chandra, V. N. Singh and S. K. Dhawan, *J. Appl. Phys.*, 2009, **106**, 044305–044311.

42 D. L. Leslie-Pelecky and R. D. Rieke, *Chem. Mater.*, 1996, **8**, 1770–1783.

43 Y.-J. Chen, P. Gao, R.-X. Wang, C.-L. Zhu, L.-J. Wang, M.-S. Cao and H.-B. Jin, *J. Phys. Chem. C*, 2009, **113**, 10061–10064.

44 V. K. Sachdev, K. Patel, S. Bhattacharya and R. P. Tandon, *J. Appl. Polym. Sci.*, 2011, **120**, 1100–1105.

45 N. C. Das, D. Das, T. K. Khastgir and A. C. Chakrraborthy, *Composites, Part A*, 2000, **31**, 1069–1081.

46 N. F. Colaneri and L. W. Shacklette, *IEEE Trans. Instrum. Meas.*, 1992, **41**, 29.

47 K. Singh, A. Ohlan, R. K. Kotnala, A. K. Bakhshi and S. K. Dhawan, *Mater. Chem. Phys.*, 2008, **112**, 651–658.

48 Y.-Y. Kim, J. Yun, Y.-S. Lee and H.-I. Kim, *Carbon*, 2011, **12**, 48–52.

49 J. Yun, J. S. Im, H.-I. Kim and Y.-S. Lee, *Colloid Polym. Sci.*, 2011, **289**, 1749–1755.

50 K. Singh, A. Ohlan, V. H. Pham, Balasubramaniyan R., S. Varshney, J. Jang, S. H. Hur, W. M. Choi, M. Kumar, S. K. Dhawan, B.-S. Kong and J. S. Chung, *Nanoscale*, 2013, **5**, 2411–2420.

51 X. Sun, J. He, G. Li, J. Tang, T. Wang, Y. Guo and H. Xue, *J. Mater. Chem. C*, 2013, **1**, 765–777.